Acta Crystallographica Section B
Structural Science
ISSN 0108-7681

Structure of a new high-pressure–high-temperature modification of antimony(III) oxide, γ-Sb_2O_3, from high-resolution synchrotron powder diffraction data

Denis Orosel,[a] Robert E. Dinnebier,[b] Vladislav A. Blatov[c] and Martin Jansen[b]*

[a]Christian Doppler Laboratory for Advanced Ferroic Oxides, Graz University of Technology, Stremayrgasse 9, Graz 8010, Austria, [b]Max Planck Institute for Solid State Research, Heisenbergstr. 1, Stuttgart 70569, Germany, and [c]Department of Chemistry, Samara State University, Ac. Pavlov St. 1, Samara 443011, Russian Federation

Correspondence e-mail: m.jansen@fkf.mpg.de

Received 17 July 2011
Accepted 5 November 2011

A quenchable new high-pressure–high-temperature modification of antimony(III) oxide, γ-Sb_2O_3, has been obtained at hydrostatic pressures of 9–11 GPa and temperatures of 573–773 K. Its crystal structure has been determined from high-resolution synchrotron powder diffraction data. γ-Sb_2O_3 consists of three-dimensionally cross-linked infinite chains of SbO_3E units (E = lone pair) with the chains forming tetragonal rod-packing. The underlying topology of γ-Sb_2O_3 (3,3T8) is found very rarely in inorganic structures; it is realised only for the polyanion $[Si_4O_4N_6]^{10-}$ that occurs in the $Ce_4(Si_4O_4N_6)O$ structure type. The structural relation to the two previously known polymorphs of Sb_2O_3 at ambient pressure, valentinite and senarmontite is discussed.

1. Introduction

In the system antimony–oxygen four different oxides, Sb_2O_3 (Dehlinger & Glocker, 1927; Bozorth, 1923; Svensson, 1974, 1975; Manohar & Gopalakrishnan, 1975; White *et al.*, 1967; Fenwick & Roberts, 1928; Hendricks & Burger, 1937), Sb_2O_4 (Pätzold *et al.*, 1962; Dihlström, 1938; Thornton, 1977; Monge *et al.*, 1988), Sb_6O_{13} (Stewart *et al.*, 1972) and Sb_2O_5 (Dehlinger, 1927; Jansen, 1978, 1979), are known to exist at ambient pressure (p = 1 bar) and temperatures up to T = 1523 K. For Sb_2O_3 two modifications have been reported: cubic α-Sb_2O_3 (senarmontite; Fig. 1) and orthorhombic β-

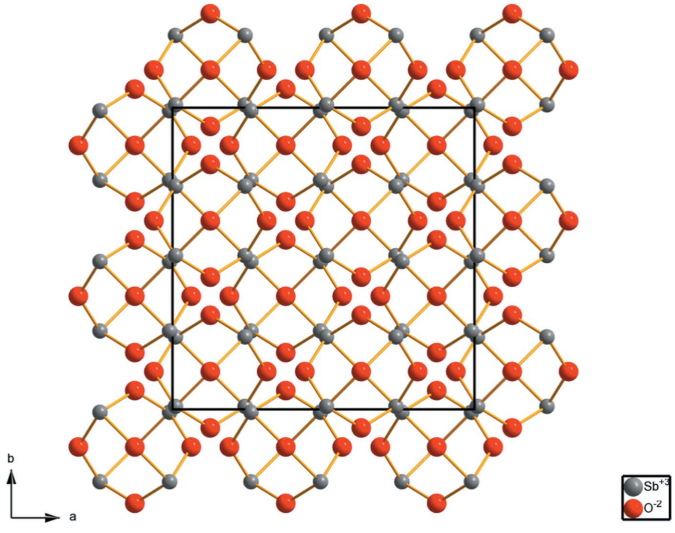

Figure 1
Packing diagram of senarmontite (α-Sb_2O_3) in $Fd\bar{3}m$ under ambient conditions in a perspective view along the c axis.

Table 1
Crystallographic and Rietveld refinement data for γ-Sb_2O_3 at ambient conditions.

Crystal data	
Chemical formula	Sb_2O_3
M_r	291.50
Crystal data, space group	Orthorhombic, $P2_12_12_1$
Temperature (K)	298
a, b, c (Å)	11.6411 (1), 7.5666 (0), 7.4771 (0)
V (Å^3)	658.61 (1)
Z	8
Radiation type	Synchrotron, λ = 0.24804 Å
Specimen shape	White powder
Data collection	
Diffractometer	Multi-analyser stage
Specimen mounting	0.3 mm capillary
Data collection mode	Continuous mode with rebinning
Scan method	Debye–Scherer
2θ values (°)	$2\theta_{min}$ = 1.0, $2\theta_{max}$ = 25.84, $2\theta_{step}$ = 0.002
Refinement	
R factors and goodness of fit	R_p = 0.043, R_{wp} = 0.067, R_{exp} = 0.021, χ^2 = 3.245
Time/scan (h)	1
No. of data points	12 420
No. of parameters	82
No. of restraints	0

Sb_2O_3 (valentinite; Fig. 2). α-Sb_2O_3 crystallizes in *Fd*3*m* (No. 227) with a = 11.1519 Å, V = 1386.91 Å^3 and Z = 16 (Bozorth, 1923; Svensson, 1975), is isotypic with cubic As_2O_3, and is stable at ambient conditions, while β-Sb_2O_3 *Pccn* (No. 56) with a = 4.911, b = 12.464, c = 5.412 Å, V = 331.27 Å^3 and Z = 4 (Svensson, 1974), is reported to exist at high temperature. According to the literature (Manohar & Gopalakrishnan, 1975; White *et al.*, 1967; Fenwick & Roberts, 1928; Hendricks & Burger, 1937), the phase transition from α- towards β-Sb_2O_3 occurs at a temperature between 843 and 879 K. Although β-Sb_2O_3 is metastable, it can exist for extended periods of time under ambient conditions (Manohar & Gopalakrishnan, 1975; Hendricks & Burger, 1937). Sb_2O_3 was investigated at hydrothermal conditions in the range up to p = 0.3 GPa and T = 973 K, but no new phases were found (White *et al.*, 1967). Since antimony(III) expresses a stereochemically active lone pair, which results in rather open structures for both known modifications of Sb_2O_3, the compound should be susceptible to pressure-driven phase transitions, as observed already for Pb_3O_4 (Dinnebier *et al.*, 2003), SeO_2 (Stahl *et al.*, 1992; Orosel *et al.*, 2004) or Bi_2O_3 (Sillen, 1941; Ghedia *et al.*, 2010). Here we report on studies using large-volume hydrostatic presses.

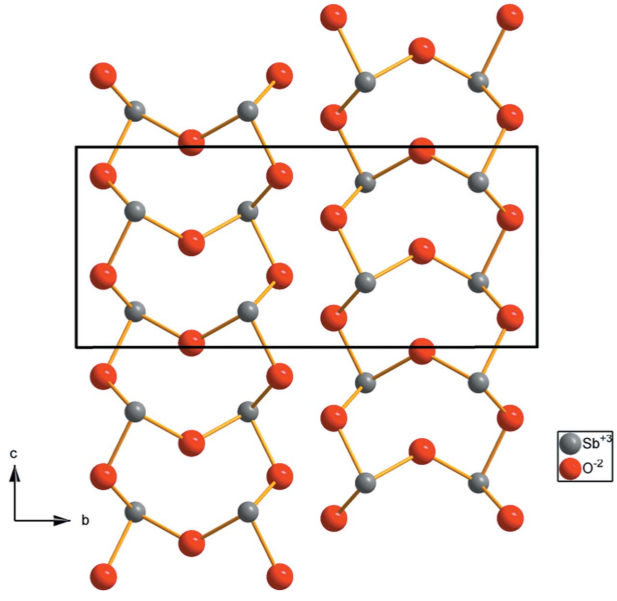

Figure 2
Packing diagram of valentinite (β-Sb_2O_3) in *Pccn* under ambient conditions in a perspective view along the *a* axis.

2. Experimental

2.1. Synthesis of the Sb_2O_3 polymorphs

Both modifications of Sb_2O_3 were used for the experiments. Commercially available α-Sb_2O_3 (Alfa Aesar 99.9%) was purified by sublimation in vacuum for 12 h applying a temperature gradient of 773 K to room temperature. β-Sb_2O_3 was synthesized according to the literature (Debray, 1866) by combining an HCl acid solution of $SbCl_3$ and a boiling Na_2CO_3 solution. The precipitate was dried at 373 K for 20 h. For both modifications, phase purity was confirmed by laboratory X-ray powder diffraction. After the drying process, both samples were filled into tightly sealed crucibles in an argon-filled glovebox. These crucibles were subjected to high pressure and high temperature in different presses (a piston cylinder press for pressures up to 2 GPa, a belt press for pressures up to 7 GPa, and a multianvil press for pressures higher than 7 GPa). At pressures between 10 and 12.5 GPa, and a temperature of 673 K, a new modification of Sb_2O_3 was found which is designated γ-Sb_2O_3 in the following.

2.2. Powder diffraction and crystal structure determination

For crystal structure determination the powder diffraction data of γ-Sb_2O_3, synthesized at p = 10 GPa and T = 673 K, were collected at the high-resolution powder diffractometer at ID31 at the European Synchrotron Radiation Facility (ESRF) (Fig. 3). An Si (111) reflection was used to select an X-ray energy of 50 keV. The size of the beam was adjusted to 2 × 0.6 mm^2 using slits. The wavelength was determined to be 0.24804 (1) Å from a silicon standard. A sample of γ-Sb_2O_3 was contained in a 0.3 mm lithium borate glass capillary, and was rotated around θ in order to improve the randomization of the crystallites. The diffracted beam was analysed with a nine-crystal analyser stage [nine Ge (111) crystals separated by 2° intervals] and detected with nine Na(Tl)I scintillation counters simultaneously. The incoming beam was monitored by an ion chamber for normalization of the decay of the primary beam. Scans were taken every 15 min at T = 298 K in continuous mode for 1 h. They were later normalized and converted to step scan data for values of 2θ from 1.0 to 25.84° in steps of 0.002°. The powder pattern contains a secondary phase which

Table 2
Selected bond distances (Å) and angles (°) of γ-Sb_2O_3 at ambient conditions.

Sb1—O2	1.88 (2)	Sb3—O4	2.04 (1)
Sb1—O5	2.05 (2)	Sb3—O3	2.04 (2)
Sb1—O1	2.24 (2)	Sb3—O2	2.11 (2)
Sb1—O2	2.72 (2)	Sb3—O3	2.52 (2)
Sb1—O1	3.08 (2)	Sb3—O5	3.17 (2)
Sb1—O4	3.34 (2)	Sb3—O2	3.18 (2)
Sb2—O1	1.87 (2)	Sb4—O6	2.00 (2)
Sb2—O4	1.91 (1)	Sb4—O5	2.06 (2)
Sb2—O6	2.06 (2)	Sb4—O3	2.08 (2)
Sb2—O1	2.66 (2)	Sb4—O6	2.59 (2)
Sb2—O5	2.91 (2)	Sb4—O3	3.03 (2)
Sb2—O6	3.19 (2)	Sb4—O4	3.32 (2)
O2—Sb1—O5	105.2 (7)	O6—Sb4—O5	98.4 (6)
O2—Sb1—O1	101.9 (7)	O6—Sb4—O3	95.7 (7)
O5—Sb1—O1	82.6 (6)	O5—Sb4—O3	82.4 (6)
O1—Sb2—O4	105.7 (6)	Sb2—O1—Sb1	111.3 (7)
O1—Sb2—O6	88.8 (7)	Sb1—O2—Sb3	128.1 (8)
O4—Sb2—O6	99.2 (7)	Sb3—O3—Sb4	125.8 (8)
O4—Sb3—O3	88.5 (5)	Sb2—O4—Sb3	133.6 (8)
O4—Sb3—O2	93.9 (6)	Sb1—O5—Sb4	125.2 (7)
O3—Sb3—O2	90.8 (6)	Sb4—O6—Sb2	131.6 (9)

could be clearly distinguished by the much broader peak width. Further experimental details are given in Table 1.

Indexing (Coelho, 2003) led to a primitive orthorhombic unit cell with lattice parameters as given in Table 1. The number of formula units per unit cell could be determined to be $Z = 8$ from volume increments. The extinctions found in the powder patterns indicated $P2_12_12_1$ as the most probable space group, which could later be confirmed by Rietveld refinement (Rietveld, 1969). The peak profiles and precise lattice parameters were determined by a LeBail fit (LeBail *et al.*, 1988) using the fundamental parameter approach of *TOPAS* Version. 4.1 (Bruker AXS, 2007; Cheary *et al.*, 2005; Coelho, 2000). From the difference curve, the powder pattern of the impurity phase was clearly visible. Nevertheless, all attempts to index the impurity phase unambiguously failed. The indexing with the highest agreement factor, describing most of the reflections, was a monoclinic unit cell in the space group $P2_1/a$ with lattice parameters of $a = 11.2745$ (2), $b = 5.6403$ (2), $c = 9.3328$ (2) Å, $\beta = 112.448$ (1)° and $V = 548.52$ (3) Å^3.

Structure determination of γ-Sb_2O_3 was performed using the program *Endeavour*, Version 1.4 (Crystal Impact GbR, 2000–2006), which combines global optimization of the difference between the calculated and measured diffraction pattern and of the potential energy of the system (Putz *et al.*, 1999).

A subsequent Rietveld refinement using *TOPAS* converged to a Bragg *R* value of 0.016. The second phase was included in the form of a Le Bail fit. Diffraction peaks in both powder patterns showed pronounced anisotropic line broadening, which was described using the phenomenological microstrain model (Stephens, 1999). Agreement factors (*R* values) are listed in Table 1, and a selection of the bond distances and angles is given in Table 2. Using the programs *PLATON* (Spek, 2003) and *K-plot* (Hundt *et al.*, 2006), no additional symmetry could be detected. The structure was also analysed using the programs *MAPLE* (Hoppe, 1979) and *TOPOS* (Blatov, 2006).

Further details on the crystal structure investigations may be obtained from the Fachinformationszentrum Karlsruhe, 76344 Eggenstein-Leopoldshafen, Germany [fax: (+49) 7247–808-666; e-mail: crysdata@fiz-karlsruhe.de], on quoting the depository number CSD-414463.

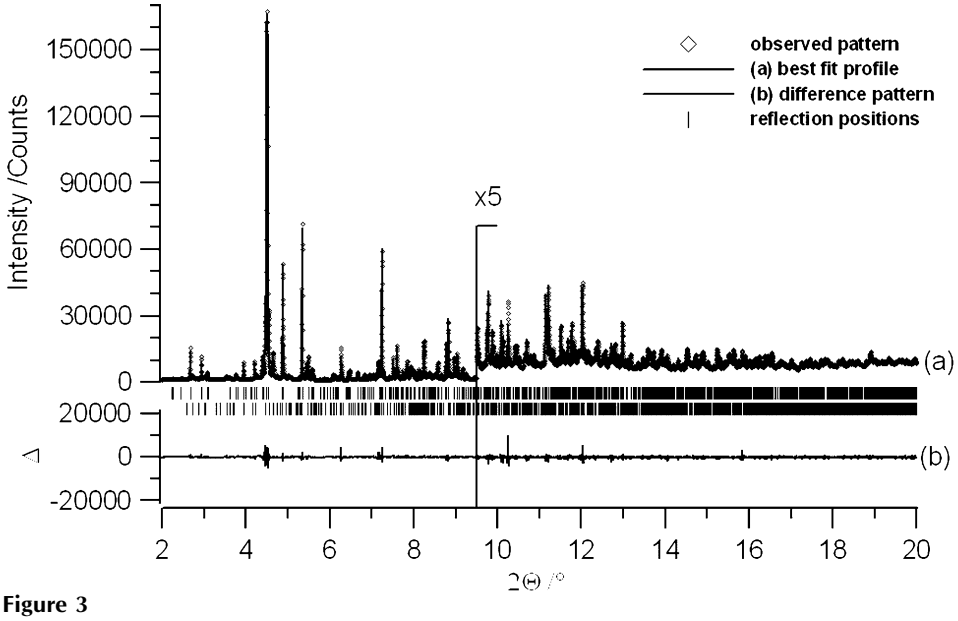

Figure 3
Scattered X-ray intensities of γ-Sb_2O_3 under ambient conditions as a function of diffraction angle 2θ. The observed pattern (diamonds) measured in Debye–Scherrer geometry, the best Rietveld fit profiles (line) and the difference curve between the observed and the calculated profiles (below) are shown. The high-angle part starting at 9.5° 2θ is enlarged for clarity. The second phase is included as a LeBail fit.

3. Results and discussion

3.1. High-pressure experiments

The results of the high-pressure experiments of Sb_2O_3 are summarized in Fig. 4. Cubic α-Sb_2O_3 is stable at ambient pressure until $T \simeq 873$ K, at $p = 2$ GPa until $T \simeq 673$ K and at $p = 15$ GPa until $T \simeq 473$ K. Outside these limits it transforms to orthorhombic β-Sb_2O_3 which stays stable up to $p = 7$ GPa and $T = 673$ K. At $p = 7$ GPa, but higher temperature, β-Sb_2O_3 disproportionates to β-Sb_2O_4 and elemental antimony. The decomposition depends strongly on the holding time. At pressures $10 \leq p \leq 12.5$ GPa and a temperature of $T = 673$ K, a new modification of Sb_2O_3, called γ-Sb_2O_3, was found. A

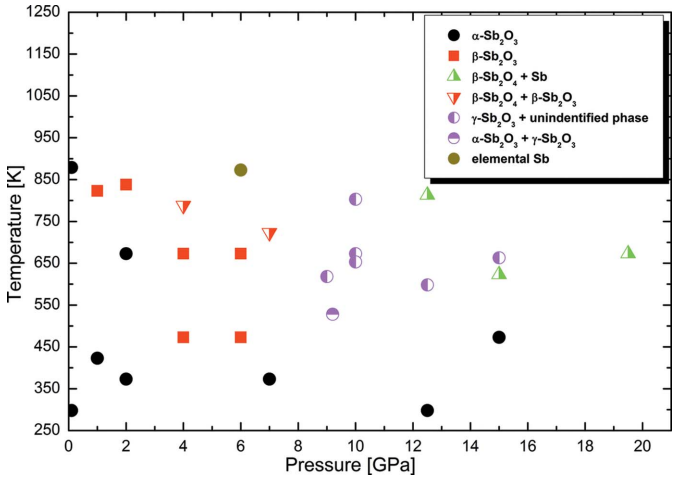

Figure 4
Phase analysis results of high T–high p preparations in the antimony–oxygen system under ambient conditions up to a temperature of 873 K and a pressure of 19.5 GPa.

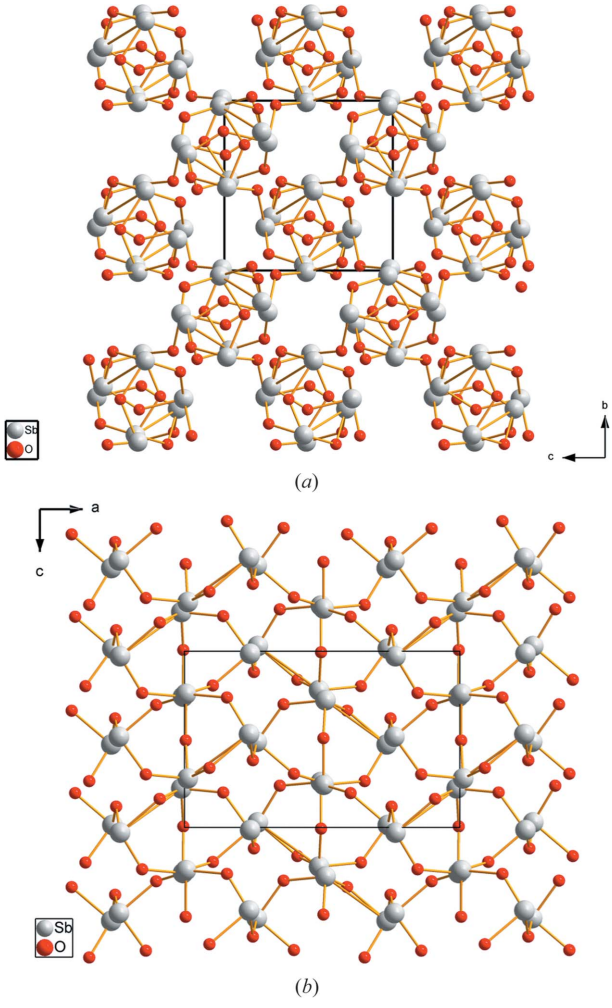

Figure 5
Packing diagram of γ-Sb_2O_3 at ambient conditions in a perspective view (*a*) along the *a* axis and (*b*) along the *b* axis.

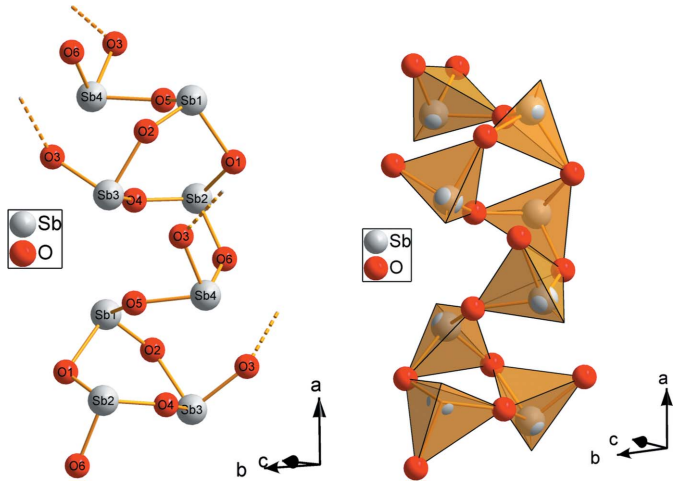

Figure 6
The four different SbO_3 trigonal pyramids (*a*) or SbO_3E tetrahedra (*b*) of γ-Sb_2O_3 and their connectivity forming a helical chain along the *a* axis at ambient conditions in a perspective view. The connections to neighboring chains are indicated by dashed lines.

second yet unknown phase was identified as a minor phase at pressures $p \simeq 10$ GPa and a major phase at a pressure of 15 GPa and a temperature of 663 K.

3.2. Crystal structure

The crystal structure of γ-Sb_2O_3 obtained at p/T conditions of 10 GPa and 673 K (Fig. 5) displays a connectivity which has not been encountered in oxides thus far. Its basic principle can be expressed by the Niggli formula $ESbO_{3/2}$, describing the coordination of antimony as a trigonal pyramid which is completed to a tetrahedron SbO_3E by considering the free electron pair (E = 5 s^2) as a pseudo-ligand. These primary building units are linked by sharing corners to form a three-dimensional framework. However, the characterization of the coordination sphere of antimony given above is very much an approximation. Using the program package *TOPOS* (Blatov, 2006), one can distinguish three different levels of Sb—O bonding corresponding to different levels of solid angles of faces of the Sb Voronoi polyhedra: 5.66, 12.77 and 17.54% of 4π steradian, or of Sb—O length 3.19, 2.66 and 2.24 Å, respectively (see the supplementary material[1]). The last level of the strongest bonding conforms to the trigonal-pyramidal coordination of antimony, while the other two levels describe weaker Sb···O interactions that are discussed below.

From Figs. 6 and 7, which show the elementary repetition unit of the three-dimensional network, one identifies cyclic secondary building units (SBU) consisting of three $Sb(1,2,3)O_3E$ pseudo-tetrahedral units. These SBUs are linked to chains by primary $Sb(4)O_3E$ units, whereas two of the linking O atoms from both primary and secondary building units are involved. The remaining third oxygen atom (O3)

[1] Supplementary data for this paper are available from the IUCr electronic archives (Reference: KD5053). Services for accessing these data are described at the back of the journal.

interlinks the resulting chains to the three-dimensional network as shown in Fig. 5.

With the *TOPOS* simplification procedures the O atoms can be contracted (transformed to edges) to obtain the underlying net (Alexandrov *et al.*, 2011), which describes the structure topology in the simplest way as a net of the antimony coordination centres (Fig. 8 top). The topology of the underlying net is known under the name 3,3T8 in the *TOPOS* TTD collection (Alexandrov *et al.*, 2011), *i.e.* as a net with two topologically different nodes of coordination 3. Since the structure of γ-Sb_2O_3 contains four non-equivalent Sb atoms, this fact indicates a topological supersymmetry in the antimony sublattice. Indeed, applying the Systre routine (Delgado-Friedrichs & O'Keeffe, 2003), the maximum symmetry $P4_132$ was found for the γ-Sb_2O_3 underlying net (that hence is chiral), and the number of non-equivalent Sb atoms was reduced to 2.

According to the *TOPOS* TTO database (Alexandrov *et al.*, 2011), the 3,3T8 topology has been found in only one structure, a metal-organic copper(II) complex (Clegg *et al.*, 2006) with the cubic symmetry $P2_13$, which is a maximal translation-equivalent subgroup of $P4_132$. To search for inorganic structures with the 3,3T8 underlying net we analysed using *TOPOS* all 6229 structure types from the ICSD (release 2011/1). The 3,3T8 topology was found only for the polyanion $[Si_4O_4N_6]^{10-}$ that occurred in the $Ce_4(Si_4O_4N_6)O$ structure type, also of the $P2_13$ symmetry (Irran *et al.*, 2000). The polyanion shows a very similar structure compared with γ-Sb_2O_3: the Si—N—Si links are topologically equivalent to the Sb—O—Sb ones, while the terminal O atoms of the $SiON_3$ tetrahedra play the stereochemical role of the *E* pairs in γ-Sb_2O_3, *i.e.* the correspondence $[Sb_4E_4O_6] \leftrightarrow [Si_4O_4N_6]^{10-}$ can be established.

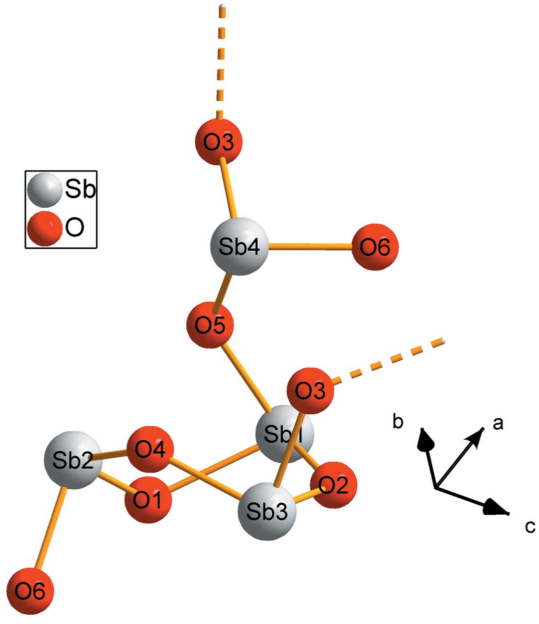

Figure 7
Twisted Sb_3O_3 ring and connected $Sb(4)O_3$ trigonal pyramid as the basic building unit of the chains (see Fig. 6) in the crystal structure of γ-Sb_2O_3 in $P2_12_12_1$ at ambient conditions in a perspective view. The connections to neighboring chains are indicated by dashed lines.

Nonetheless, γ-Sb_2O_3 is the first case where the 3,3T8 underlying net describes the whole structure topology.

The 3,3T8 underlying net can be more simplified if one considers the cyclic SBUs as a whole by representing them as their centres of gravity. The resulting net (Fig. 8 middle) is uninodal (with one topologically non-equivalent node), is

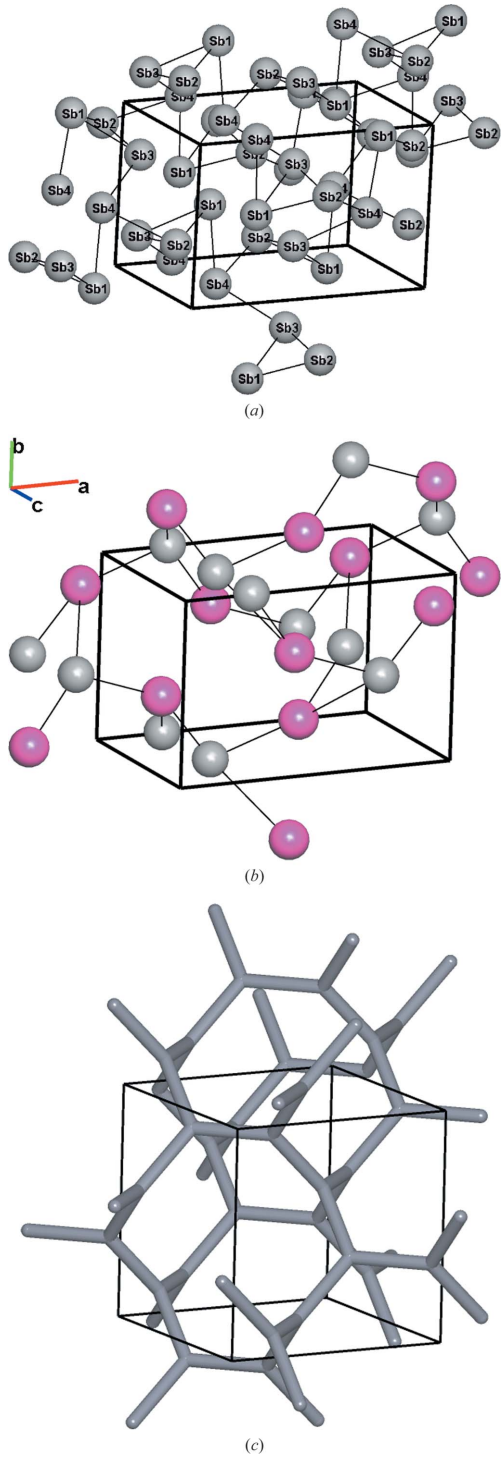

Figure 8
γ-Sb_2O_3 underlying net of the 3,3T8 topology (*a*), the corresponding **srs** net (*b*), and the **srs** net in the most symmetric ($I4_132$) embedding (*c*). The positions of the magenta balls coincide with the centres of gravity of the triangular SBUs.

Table 3
Bond-valence sums for γ-Sb_2O_3 (with and without consideration of van der Waals radii).

Atoms	Sb1	Sb2	Sb3	Sb4		
Bond-valence sum†	2.36	2.92	2.22	2.39		
Bond-valence sum‡	2.64	3.28	2.61	2.66		
Atoms	O1	O2	O3	O4	O5	O6
Bond-valence sum†	1.63	1.77	1.49	1.82	1.50	1.59
Bond-valence sum‡	1.90	2.00	1.84	1.91	1.67	1.88

† Without van der Waals radii. ‡ With van-der-Waals-radii

called **srs**, and describes the Si net in α-$SrSi_2$ (Fig. 8 bottom) as well as many other topological motifs of different chemical natures (Hyde *et al.*, 2008). Thus, the 3,3T8 net can be described as a 'half-augmented' **srs**, *i.e.* the **srs** net where half of the nodes are augmented with triangles.

Considering the next three longer Sb—O distances up to 3.35 Å (which is still shorter as the sum of the van der Waals radii of 2.06 + 1.52 Å), additional stabilization of the crystal

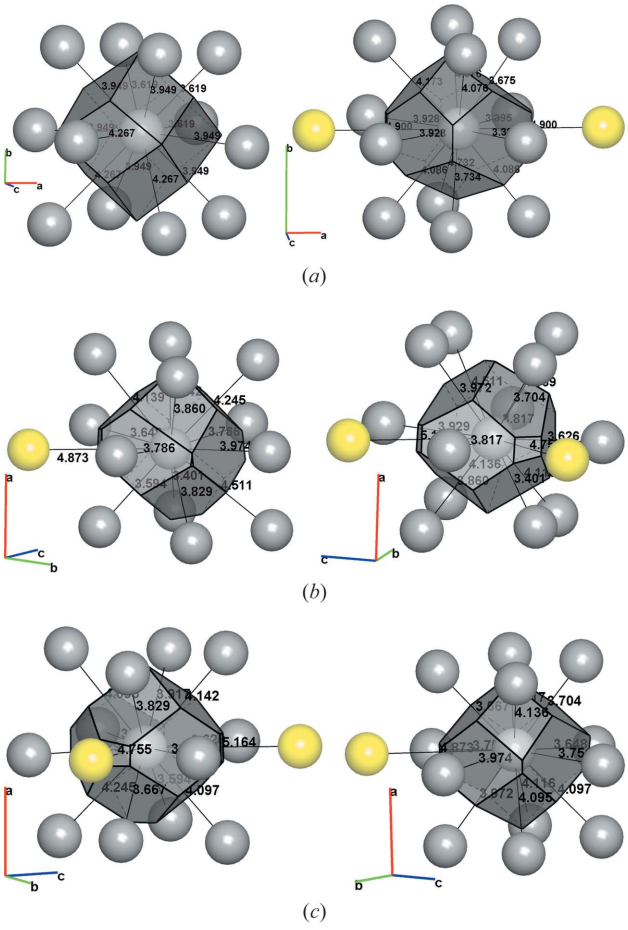

Figure 9
Voronoi polyhedra for Sb atoms in the antimony sublattice: (*a*) Sb1 in α-Sb_2O_3 and Sb1 in β-Sb_2O_3; (*b*) Sb1 and Sb2, and (*c*) Sb3 and Sb4 in γ-Sb_2O_3. 12 grey Sb atoms form a distorted cuboctahedral environment; yellow distant Sb atoms give rise to additional minor faces of the Voronoi polyhedra due to the sublattice distortion. This figure is in colour in the electronic version of this paper.

Table 4
Overview of the motives of the mutual allocation, the effective coordination number (ECoN), and the mean fictive ionic radii (MEFIR; pm) for the three modifications of Sb_2O_3.

					ECoN	MEFIR
α-Sb_2O_3						
	Sb					
O	3/2				2.0	140
ECoN	3.0					
MEFIR	58					
β -Sb_2O_3						
	Sb					
O1	1/2				2.2	144
O2	2/2				2.1	142
ECoN	3.2					
MEFIR	59					
γ-Sb_2O_3						
	Sb1	Sb2	Sb3	Sb4		
O1	1/1	1/1	–	–	1.4	145
O2	1/1	–	1/1	–	2.0	142
O3	–	–	1/1	1/1	2.2	144
O4	–	1/1	1/1	–	2.0	141
O5	1/1	–	–	1/1	1.9	147
O6	–	1/1	–	1/1	1.9	146
ECoN	2.3	2.8	3.2	3.1		
MEFIR	51	49	65	62		

structure of γ-Sb_2O_3 is achieved due to the contribution of these bonds to the bond-valence sum (Sidey, 2010) of the participating antimony–oxygen atoms (Table 3).

The crystal structures of γ-Sb_2O_3 and β-Sb_2O_3 show similarities in the sense that in β-Sb_2O_3 linked Sb_2O_3 units form infinite chains along the *c* axis. Parallel chains in γ-Sb_2O_3 are arranged in tetragonal rod packing (O'Keeffe & Andersson, 1977), in contrast to β-Sb_2O_3 where hexagonal rod packing is realised (Fig. 2). Both crystal structures are related *via* $P2_12_12$ as an intermediate space group, allowing primary and secondary distortion modes.

An important similarity between all Sb_2O_3 modifications is that the Sb atoms form a distorted face-centered cubic sublattice. This is evident from the analysis of their Voronoi polyhedra (Fig. 9), which show a distinct cuboctahedral environment; the resulting 12-coordinated net has the **fcu** (face-centered cubic) topology. Thus, the phase transitions keep the Sb motif topologically the same; the changes mainly consist of geometrical distortions and shifts of O atoms.

The motifs of the mutual allocation, the effective coordination number (ECoN) and the median fictive ionic radii (MEFIR; Hoppe, 1979) were calculated for all three polymorphs of Sb_2O_3 (Table 4). They are quite similar for O and Sb atoms. The Madelung fraction of the lattice energy (Hoppe, 1970*a*,*b*) is of the same order of magnitude for identical ions. The Coulomb fraction of the lattice energy is very similar for all three modifications of Sb_2O_3, whereas the energy of the high-pressure phase lies between the values of the known phases (Table 5). The slightly higher value for the lattice energy in the case of γ-Sb_2O_3 compared with α-Sb_2O_3 can be understood by the shorter Sb—O distances in the high-pressure phase.

Table 5
Comparison of the MAPLE values (kJ mol^{-1}) for the three modifications of Sb_2O_3.

Atom	MAPLE (α-Sb_2O_3)	MAPLE (β-Sb_2O_3)	MAPLE (γ-Sb_2O_3)
Sb1	2318.7 (4×)	2284.0 (4×)	2169.6
Sb2	–	–	2370.0
Sb3	–	–	2186.1
Sb4	–	–	2250.5
O1	942.5 (6×)	1052.5 (2×)	1039.7
O2	–	945.3 (4×)	1096.4
O3	–	–	1019.3
O4	–	–	951.9
O5	–	–	939.8
O6	–	–	988.3
	Σ = 14 930 kJ mol^{-1}	Σ = 15 022 kJ mol^{-1}	Σ = 15 012 kJ mol^{-1}

Table 6
Comparison of the volumes for the three modifications of Sb_2O_3.

	α-Sb_2O_3	β-Sb_2O_3	γ-Sb_2O_3
Unit cell volume (Å^3)	1386.91	331.27	658.61
Volume per formula unit (Å^3)	86.68	82.82	82.33
Molecular volume (cm^3 mol^{-1})	52.21	49.88	49.59

Comparing the unit cell and the molecular volumes of all three Sb_2O_3 phases, it is clearly seen that the γ-phase possesses the smallest volume of the three modifications, as is expected for a high-pressure phase (Table 6). Whereas the volume of β-Sb_2O_3 is only about 0.6% larger than that of γ-Sb_2O_3, the difference between the β and α phases is $\sim$ 4.6%.

Other A_2X_3 structures like Sb_2S_3 (Hofmann, 1933; Bayliss & Nowacki, 1972) show similarities with γ-Sb_2O_3. The structure of Sb_2S_3 is built by infinite columns of Sb_4S_6 units along the *b* axis. Despite the infinite chains the main difference to γ-Sb_2O_3 is that the chains are not directly connected to each other. The columns form sheets perpendicular to the *a* axis with interatomic distances of 3.167 Å. These sheets again are held together by interatomic bonds between 3.373 and 3.642 Å, which are all considerably shorter than the van der Waals radii sum for Sb and S of 4.05 Å. High-pressure data of Sb_2S_3 up to p = 10 GPa in a diamond–anvil cell only revealed a change of the coordination polyhedra of the two Sb atoms with increasing pressure but no phase transition (Lundegaard *et al.*, 2003). The high-pressure coordination of Sb_2S_3 resembled more the coordination of Bi_2S_3 at ambient pressure.

Financial support by the Bundesministerium für Bildung und Forschung (BMBF), and the Fonds der Chemischen Industrie (FCI) is gratefully acknowledged. Special thanks go to Andy Fitch (ESRF) for his help during data collection.

References

Alexandrov, E. V., Blatov, V. A., Kochetkov, A. V. & Proserpio, D. M. (2011). *CrystEngComm*, **13**, 3947–3958.

Amador, J., Gutierrez Puebla, E., Monge, M. A., Rasines, I. & Ruiz Valero, C. (1988). *Inorg. Chem.* **27**, 1367–1370.

Bayliss, P. & Nowacki, W. (1972). *Z. Kristallogr.* **135**, 308–315.

Blatov, V. A. (2006). *IUCr CompComm Newsl.* **7**, 4–38, http://www.topos.ssu.samara.ru.

Bozorth, R. M. (1923). *J. Am. Chem. Soc.* **45**, 1621–1627.

Bruker (2007). *TOPAS*, Version 4.1. Bruker AXS, Karlsruhe, Germany.

Cheary, R. W., Coelho, A. A. & Cline, J. P. (2004). *J. Res. Natl. Inst. Stand. Technol.* **109**, 1–25.

Clegg, J. K., Lindoy, L. F., Mcmurtrie, J. C. & Schilter, D. (2006). *Dalton Trans.* pp. 3114–3121.

Coelho, A. A. (2000). *J. Appl. Cryst.* **33**, 899–908.

Coelho, A. A. (2003). *J. Appl. Cryst.* **36**, 86–95.

Crystal Impact GbR (2000–2006). *Endeavour*, Version 1.4. Crystal Impact GbR, Bonn, Germany.

Debray, H. (1866). *J. Prakt. Chem.* **98**, 151–153.

Dehlinger, U. (1927). *Z. Kristallogr.* **66**, 108–119.

Dehlinger, U. & Glocker, R. (1927). *Z. Anorg. Allg. Chem.* **165**, 41–45.

Delgado-Friedrichs, O. & O'Keeffe, M. (2003). *Acta Cryst.* A**59**, 351–360, http://www.gavrog.org.

Dihlström, K. (1938). *Z. Anorg. Allg. Chem.* **239**, 57–64.

Dinnebier, R. E., Carlson, S., Hanfland, M. & Jansen, M. (2003). *Am. Mineral.* **88**, 996–1002.

Fenwick, F. & Roberts, J. (1928). *J. Am. Chem. Soc.* **50**, 2125–2147.

Ghedia, S., Locherer, T., Dinnebier, R. E., Prasad, D. L. V. K., Wedig, U., Jansen, M. & Senyshyn, A. (2010). *Phys. Rev. B*, **82**, 024106.

Gopalakrishnan, P. S. & Manohar, H. (1975). *J. Solid State Chem.* **15**, 61–67.

Hendricks, S. B. & Burger, M. J. (1937). *J. Chem. Phys.* **5**, 600.

Hofmann, W. (1933). *Z. Kristallogr.* **86**, 225–245.

Hoppe, R. (1970*a*). *Angew. Chem.* **82**, 7–16.

Hoppe, R. (1970*b*). *Angew. Chem. Int. Ed. Engl.* **9**, 25–34.

Hoppe, R. (1979). *Z. Kristallogr.* **150**, 23–52.

Hundt, R., Schön, J. C. & Jansen, M. (2006). *J. Appl. Cryst.* **39**, 6–16.

Hyde, S. T., O'Keeffe, M. & Proserpio, D. M. (2008). *Angew. Chem. Int. Ed.* **47**, 7996–8000.

Irran, E., Koellisch, K., Leoni, S., Nesper, R., Henry, P. F., Weller, M. T. & Schnick, W. (2000). *Chem. Eur. J.* **6**, 2714–2720.

Jansen, M. (1978). *Angew. Chem.* **90**, 141–142.

Jansen, M. (1979). *Acta Cryst.* B**35**, 539–542.

LeBail, A., Duroy, H. & Fourquet, J. L. (1988). *Mater. Res. Bull.* **23**, 447–452.

Lundegaard, L. F., Miletich, R., Balic Zunic, T. & Makovicky, E. (2003). *Phys. Chem. Miner.* **30**, 463–468.

O'Keeffe, M. & Andersson, S. (1977). *Acta Cryst.* A**33**, 914–923.

Orosel, D., Leynaud, O., Balog, P. & Jansen, M. (2004). *J. Solid State Chem.* **177**, 1631–1638.

Pätzold, H., Strunz, H. & Gründer, W. (1962). *Neues Jahrb. Miner. Abh.* **5**, 93–98.

Putz, H., Schön, J. C. & Jansen, M. (1999). *J. Appl. Cryst.* **32**, 864–870.

Rietveld, H. M. (1969). *J. Appl. Cryst.* **2**, 65–71.

Sidey, V. (2010). *Acta Cryst.* B**66**, 307–314.

Sillen, L. G. (1941). *Z. Kristallogr.* **103**, 274–290.

Spek, A. L. (2003). *J. Appl. Cryst.* **36**, 7–13.

Stahl, K., Legros, J. P. & Galy, J. (1992). *Z. Kristallogr.* **202**, 99–107.

Stephens, P. W. (1999). *J. Appl. Cryst.* **32**, 281–289.

Stewart, D. J., Knop, O., Ayasse, C. & Woodhams, F. D. W. (1972). *Can. J. Chem.* **50**, 690–700.

Svensson, C. (1974). *Acta Cryst.* B**30**, 458–461.

Svensson, C. (1975). *Acta Cryst.* B**31**, 2016–2018.

Thornton, G. (1977). *Acta Cryst.* B**33**, 1271–1273.

White, W. B., Dachille, F. & Roy, R. (1967). *Z. Kristallogr.* **125**, 450–458.